

This is a repository copy of *In-situ ultrasonic shear wave sensing of thin metallic coatings* on journal bearing shells.

White Rose Research Online URL for this paper: https://eprints.whiterose.ac.uk/id/eprint/230047/

Version: Published Version

Article:

Wu, L., Palamarciuc, I., Bajwa, R. et al. (2 more authors) (2025) In-situ ultrasonic shear wave sensing of thin metallic coatings on journal bearing shells. Friction. ISSN: 2223-7690

https://doi.org/10.26599/frict.2025.9441160

Reuse

This article is distributed under the terms of the Creative Commons Attribution (CC BY) licence. This licence allows you to distribute, remix, tweak, and build upon the work, even commercially, as long as you credit the authors for the original work. More information and the full terms of the licence here: https://creativecommons.org/licenses/

Takedown

If you consider content in White Rose Research Online to be in breach of UK law, please notify us by emailing eprints@whiterose.ac.uk including the URL of the record and the reason for the withdrawal request.

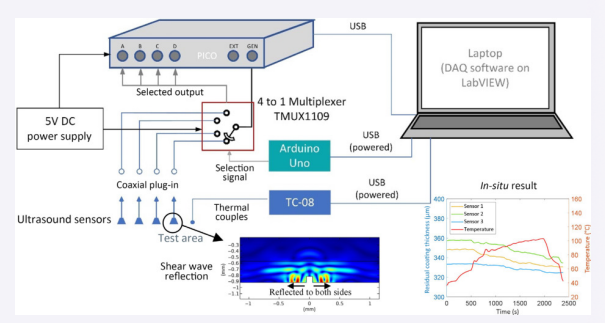


In-situ ultrasonic shear wave sensing of thin metallic coatings on journal bearing shells

Liqun Wu¹, Ion Palamarciuc^{2,\infty}, Rizwan Sarwar Bajwa², Yi Zhang³, Rob S. Dwyer-Joyce^{1,\infty}

Site this article: Wu LQ, Palamarciuc I, Bajwa RS, et al. Friction 2025, 13: 9441160. https://doi.org/10.26599/FRICT.2025.9441160

ABSTRACT: Ultrasonic testing using shear polarised waves is widely applied in medical and engineering fields, commonly employed for hardness or stress measurement. The advantage of ultrasonic shear waves for wear measurement lies in their lower wave propagation speed and their sensitivity in measuring the wear scars formed through the shear motion. An *in-situ* wear measurement method of thin metallic coatings using ultrasonic shear waves is proposed in this study. A finite element analysis was used to investigate the interaction between an ultrasonic shear wave and various geometric wear scars. Compared with longitudinal waves, the result shows that 10 MHz shear



waves and 22 MHz longitudinal waves have a similar performance in the measurement of undamaged metallic coatings. Whereas, for discontinuously distributed scars, the 10 MHz shear wave shows an amplitude decrease, where the energy has been reflected to both sides. Then, the *in-situ* tests were conducted, and the shear wave measurements of wear were compared with the microscope results. For 350 µm aluminium-alloy coated samples, the maximum deviation between shear wave results and microscope results was 5.13 µm, with a relative error of 1.5%. For 250 µm bronze–lead coatings, the maximum deviation was 5.54 µm, with a relative error of 2.51%. The practicality of using shear waves to determine continuous wear progression in bearings is briefly discussed, and their potential for monitoring the health of bearing coatings in service.

KEYWORDS: ultrasonic shear wave; non-destructive testing; surface wear measurement; metallic coatings; journal bearings

1 Introduction

Ultrasonic bulk wave testing has been commonly used in various fields. The biggest advantage of bulk wave testing lies in its applicability to various materials and structures, especially its non-destructive nature. Ultrasonic shear waves can be generated either from a shear-polarized piezo or by mode conversion of a longitudinal wave through a wedge probe, both useful for surface or sub-surface detection [1]. Current practical applications of shear wave testing are primarily focused on human tissues and metal materials, which can be divided into shear wave elastography and shear wave attenuation measurement [2–4].

When ultrasonic waves are obliquely incident on an interface, mode conversion occurs, splitting the waves into longitudinal and shear components. The relationship between axial stress and wave speed in axisymmetric cylindrical solids was investigated and applied to estimate axial stresses in high-tension bolts [5, 6]. The shear and elastic moduli of materials can be calculated from the velocities of ultrasonic longitudinal and shear waves, and used to examine the microstructure of different steel types [7]. As an

anisotropic medium, the propagation of ultrasound in human bone is complex. A model based on the finite-difference time-domain method has been established, treating the bone plate as an isotropic medium. It was demonstrated that along the bone axis direction, the measurement of ultrasonic shear wave velocity is consistent with the model results [8]. Stress and strain have also been measured based on the relationship between the shear/elastic modulus and wave speed [9]. An electromagnetic-based measurement was used to determine the longitudinal-to-shear wave speed ratio to obtain the residual stress in aluminium plate structures when the thickness was unknown [10].

The generation of shear waves in metal materials is often achieved through laser or electromagnetic acoustic transducers (EMAT). Research shows that a laser source can generate shear waves, while an EMAT receives the reflected waves. This laser–EMAT setup can measure the thickness of a 0.4 mm steel plate with a relative error of less than 4% compared to the metallographic method [11]. Polarized shear waves generated by EMAT can also detect crack-like defects based on finite element simulations [12]. However, there is limited research on using

[©] The Author(s) 2025. This is an open access article under the terms of the Creative Commons Attribution 4.0 International License (CC BY 4.0, http://creativecommons.org/licenses/by/4.0/).



¹Leonardo Centre for Tribology, School of Mechanical, Aerospace and Civil Engineering, The University of Sheffield, Sheffield S10 2TN, UK. ²Daido Metal Co., Ltd., European Technical Centre (UK), Ilminster, Somerset TA19 9PH, UK. ³Daido Metal Co., Ltd., Technology Division, Tendoh Shinden, Maehara, Inuyama, Aichi 484-0061, Japan.

应 Corresponding authors. E-mail: I. Palamarciuc, Ion.Palamarciuc@daidometal.com; R. S. Dwyer-Joyce, r.dwyer-joyce@sheffield.ac.uk Received: November 21, 2024; Revised: June 22, 2025; Accepted: August 1, 2025

shear waves for coating thickness or wear tests, as well as for realtime monitoring systems.

In previous research, ultrasonic longitudinal waves have been used for residual thickness and in-situ wear testing of metallic bearing coatings [13, 14]. It was shown that piezoelectric sensors generating 22 MHz longitudinal waves can effectively achieve insitu measurement under various bearing operating conditions. For the same material, the speed of shear waves is about half that of longitudinal waves, which means that shear waves theoretically have a higher spatial resolution in thickness testing than longitudinal waves of the same frequency. Moreover, friction between the coating and shaft works as a shear motion, while the wear scars distribute as some scratches along the circumferential direction. These discontinuous scars may affect the shear motion between particles during shear wave propagation. In this work, ultrasonic shear waves for coating thickness and wear measurement are studied, and the required theories, modelling, and *in-situ* measurement are presented.

2 Principle of shear wave measurement

2.1 Propagation of ultrasonic shear wave

For ultrasonic shear waves, the vibration direction of particles in the medium is perpendicular to the direction of ultrasound propagation, as shown in Fig. 1. The particles vibrate in a shear motion due to the shear stress between them. The speed of sound for longitudinal wave $c_{\rm L}$, and shear wave $c_{\rm T}$, in solid materials can be expressed in terms of Young's modulus E, density ρ , and Poisson's ratio v, as given by Eqs. (1) and (2) [15].

$$c_{\rm L} = \sqrt{\frac{E}{\rho}} \cdot \sqrt{\frac{1-\nu}{(1+\nu)(1-2\nu)}} \tag{1}$$

$$c_{\rm T} = \sqrt{\frac{E}{\rho}} \cdot \sqrt{\frac{1-\nu}{2(1+\nu)}} \tag{2}$$

The propagation of shear waves relies on the transmission of shear displacement between particles. However, there is almost no shear stress between particles in a fluid, leading to a significant attenuation of the shear wave. Thus, immersion testing is not viable; for *in-situ* measurement of bearing coatings, the sensor is permanently bonded on the bearing outer face with a thin epoxy coupling layer to enable the transmission of shear waves.

2.2 Pulse-echo technique

The pulse-echo method is used for real-time coating thickness measurement; each sensor acts as both signal transmitter and receiver. When the transmitted shear wave encounters the coating-steel interface and then the coating-lubricant interface, two reflections occur. The coating thickness, d, can be obtained from the time-of-flight (ToF) between the two reflected signals. The coating thickness d is then given by Eq. (3):

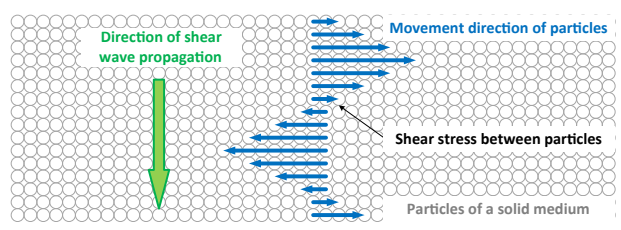


Fig. 1 Diagram of shear wave propagation in a solid medium.



$$d = c(T)\Delta t/2 \tag{3}$$

where the speed of sound c is a function of temperature T; Δt represents the ToF between reflections from either side of the coating. The reflection positions are determined by the peak positions of the reflection pulses.

2.3 Determining of time-of-flight

For coating materials with an acoustic impedance significantly different from steel, the ToF can be determined from the difference in the time-of-arrival (ToA) of two reflections from either side of the coating. The time of energy arrival was used as the estimator of interface location for echo signals in Ref. [16]. For coating materials with a similar acoustic impedance to steel, such as bronze–lead (Bz–Pb) coatings, a "reflection package" method based on analytic signal and Hilbert transform was used, as shown in Fig. 2 [14]. Meanwhile, the energy-based analysis can effectively eliminate the influence of ultrasound scattering at lead phases.

In Fig. 2(a), A and B represent the steel–coating and coating–lubricant interface. A_1 and A_2 are the first and second reflection from interface A, while B_1 and B_2 are the first and second reflection from interface B. $ToA^{(B_1)}$ and $ToA^{(A_1)}$ are the ToAs of the first reflection of interface B and interface A.

Before bearing service, calibration is performed to obtain the thickness of the undamaged coating at room temperature. $C_{\rm B}\left(T|t=0\right)$ is the speed of sound in the Bz–Pb coating during calibration. In general, it is necessary to record the ToF between A_1 and B_1 before the operation, to obtain the initial coating thickness h_2 .

$$h_2 = \frac{\left(\text{ToA}^{(B_1)} - \text{ToA}^{(A_1)}\right) C_B(T|_{t=0})}{2}$$
 (4)

During shaft rotation, $c_s(T)$ and $c_B(T)$ are the speeds of sound in steel and Bz–Pb, respectively, both functions of temperature T. Both increase due to frictional heating, and the coating starts to wear, usually shown as a reduction in Δh . The expression of Δh can be derived via Eq. (5):

$$\left[\text{ToF}^{(B)} - \frac{2(h_2 - \Delta h)}{c_B(T)} \right] c_S(T) = \left(\text{ToF}^{(B|_{t=0})} - \frac{2h_2}{C_B(T|_{t=0})} \right) \cdot C_S(T|_{t=0})$$
(5)

In Eq. (5), $C_{\rm S}(T|t=0)$ is the speed of sound in steel during the calibration. ${\rm ToF^{(B)}}={\rm ToA^{(B_2)}}-{\rm ToA^{(B_1)}}$ is the ToF of "reflection package", and ${\rm ToF^{(B|t=0)}}$ is the ToF of "reflection package" during calibration.

3 Simulation of ultrasonic shear wave propagation in metal layers

3.1 Background of simulation

An ultrasonic shear wave was used as input to study the interaction between shear waves and the bearing coating wear. However, the highest center frequency of commercially available shear-mode piezo-elements is much lower than that of longitudinal-mode ones. The common high-frequency range for lead zirconate titanate (PZT) material is around 22 MHz for longitudinal sensors and 10 MHz for shear sensors. Therefore, it is necessary to compare the performance of 10 MHz shear wave with the 22 MHz longitudinal wave and investigate the measurement capability of 10 MHz shear wave before actual testing.

Figures 3(a) and 3(b) show the wear scars on aluminium-alloy coating and bronze–lead coated bearings after operation. The shape of wear typically distributes circumferentially and starts from independent scratches. Since the propagation of a shear wave relies on shear stress, it can be assumed that the shear waves are more sensitive to these discontinuities along the surface, especially along the axial direction. Figures 3(c) and 3(d) depict the surface wear on aluminium-alloy and bronze–lead coatings, serving as the references for modelling.

The finite element analysis was performed using the elastic wave module of COMSOL Multiphysics. The Navier equation was used as the governing equation, expressed as a function of Young's modulus E, Poisson's ratio ν , density ρ , and time t, as Eq. (6). In Eq. (6), ∇ is the Hamiltonian operator used for vector differentiation. The zero displacement and zero velocity were set as initial conditions.

$$\frac{E}{2(1+\nu)} \left[\nabla^2 \mathbf{u} + \frac{1}{1-2\nu} \nabla (\nabla \cdot \mathbf{u}) \right] + \mathbf{F} = \rho \frac{\partial^2 \mathbf{u}}{\partial t^2}$$
 (6)

The displacement and boundary load are in vector form, \mathbf{u} and \mathbf{F} . The amplitude of ultrasound input is expressed as Eq. (7), while f is the signal frequency:

$$|F| = (1 - \cos(2\pi f t/3)) \sin(2\pi f t)$$
 (7)

All the boundaries, except the input boundary, were set as free. The input region was set for two different wave modes and also used as the probe to receive the reflected signals. For this simulation, the materials were set as steel, pure aluminum, and copper, instead of the actual bearing alloys (this is due to the difficulty in obtaining the properties of the real alloys with varying compositions). Table 1 shows the parameters of materials used in the modelling.

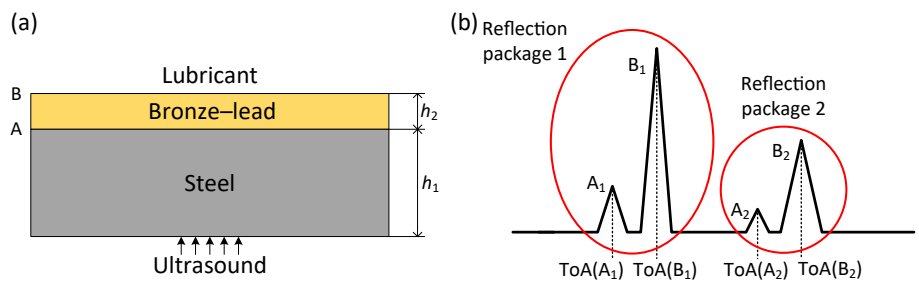


Fig. 2 (a) Diagram of a double-layer structure of a bronze-lead coated bearing shell. (b) Diagram of "reflection package" method for analyzing reflection signals.

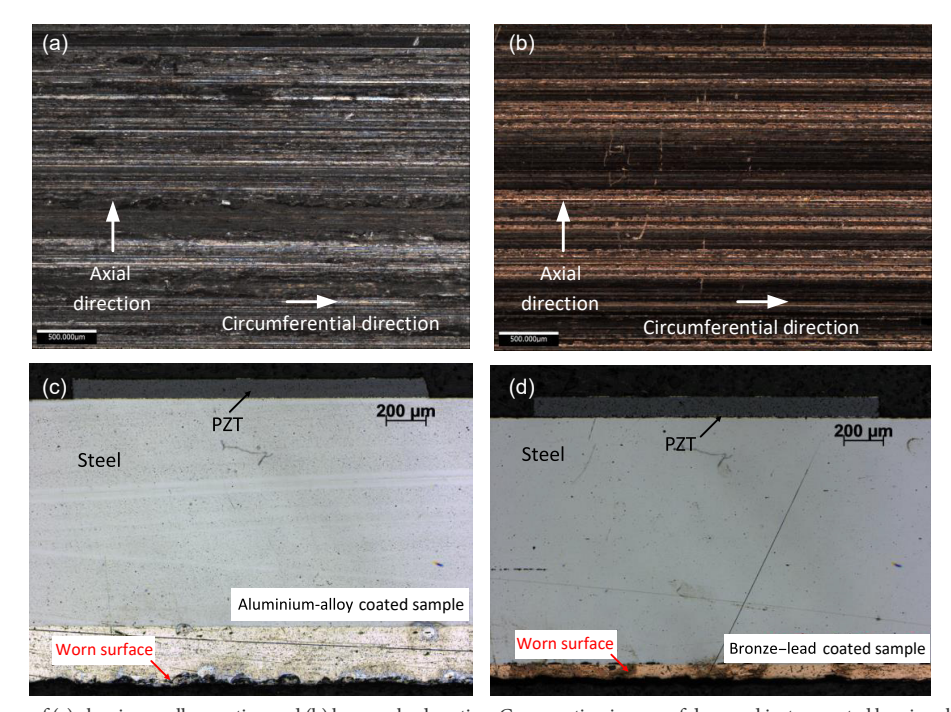


Fig. 3 Damaged surfaces of (a) aluminum-alloy coating and (b) bronze-lead coating. Cross-section images of damaged instrumented bearing shell: (c) aluminium-alloy coating and (d) bronze-lead coating.

Table 1 Properties of materials in shear wave modelling

Description	Density (g/cm³)	Thickness (mm)	Width (mm)	Young's modulus (GPa)	Poisson's ratio
Steel bearing layer	7.85	1.14	5	205	0.28
Aluminum coating	2.70	0.35	5	70	0.33
Copper coating	8.96	0.25	5	110	0.35
Ultrasound input area	_	_	2	_	

3.2 Comparison between longitudinal wave and shear wave

Double-layer structure models were established, as shown in Fig. 4, including steel–aluminum and steel–copper combinations. The blue lines represent the ultrasound input area (2 mm wide), with the vibration direction marked. The input load was set as along the *y*-direction for longitudinal wave, while the *x*-direction for shear wave. The perfect matched layer (PML) was used to simulate an infinite absorbing space. The grid size for meshing was set to $10{\text -}20~\mu\text{m}$, $1/10{\text -}1/5$ of the shortest wavelength, corresponding to the wavelength of a 22 MHz shear wave in copper.

The comparison results between 22 MHz longitudinal wave and 10 MHz shear wave are shown in Fig. 5. The probe displacement in the *x*-direction was plotted for shear wave models, and in the *y*-direction for longitudinal wave models. The red curve represents the signal (A-scan) of the 22 MHz longitudinal wave, and the blue curve represents the 10 MHz shear wave. Pulses 1 and 2 marked in Fig. 5 represent the coating-steel and coating-air reflections, respectively.

In Figs. 5(a) and 5(b), the 22 MHz longitudinal wave and 10 MHz shear wave have been compared in both aluminium and copper coating respectively. It can be observed that the ToF between shear wave reflections is greater than that of longitudinal wave reflections due to the slower shear wave speed. In aluminum coating, the ToF values between two coating interface reflections are 0.116 and 0.224 μs for longitudinal and shear waves, respectively. In copper coating, the ToF values are 0.114 and 0.232 μs . Two distinct reflected pulses can be observed in both materials, which means that the 10 MHz ultrasonic shear wave can distinguish the two interfaces of both the 350 μm aluminium coating and the 250 μm copper coating in the numerical model.

3.3 Simulation of wear measurement using shear wave

Figure 6(a) shows the simulation diagram, and Figs. 6(b) and 6(c) depict the simulation results using a 10 MHz shear wave to measure a 2 mm-wide, 0.1 mm-deep surface damage on a 350 μm -thick aluminium coating and a 2 mm-wide, 0.1 mm-deep surface damage on a 250 μm -thick copper coating. The red curve corresponds to the undamaged surface, and the blue curve corresponds to the damaged surface.

From both aluminum and copper models, the reflection signal at the coating–steel interface remains unchanged when the wear exists. However, the coating-air reflection from a damaged surface arrives earlier than that of the undamaged surface. Based on the simulation results, it is feasible to use ultrasonic shear waves to detect the changes in coating thickness.

A simulation measuring independent scratches was also investigated, where the size of each damage was set to 0.1 mm deep and 0.1 mm wide, as shown in Fig. 7(a). The ability between longitudinal wave and shear wave were compared. The results are shown in Figs. 7(b)–7(d).

Based on the simulation results in Fig. 7, when using the 22 MHz longitudinal wave to detect the scars on the aluminum coating, the amplitude is reduced by 39%. For copper coating, the amplitude is reduced by 35%. When using the 10 MHz shear wave, the reflection from the scars on aluminum coating has reduced by 70%, and by 46% for copper coating. The reflected signal of shear waves exhibits a significant amplitude change, especially in the aluminium coating.

In solid media, shear wave propagates "layer by layer". When a layer of particles is discontinuous, it will be reflected to both sides. Figure 8 shows the displacement of the medium when the longitudinal and shear wave is reflected from a 0.1 mm-wide,

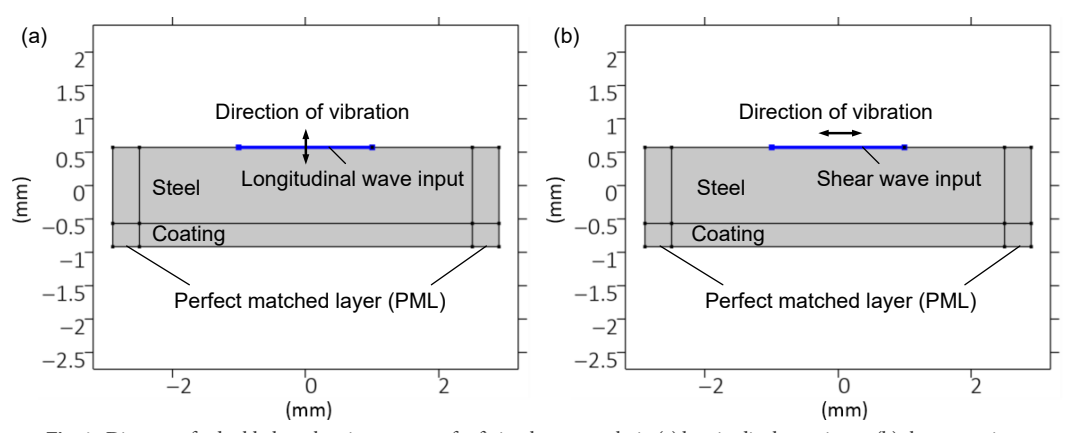


Fig. 4 Diagram of a double-layer bearing structure for finite element analysis: (a) longitudinal wave input; (b) shear wave input.

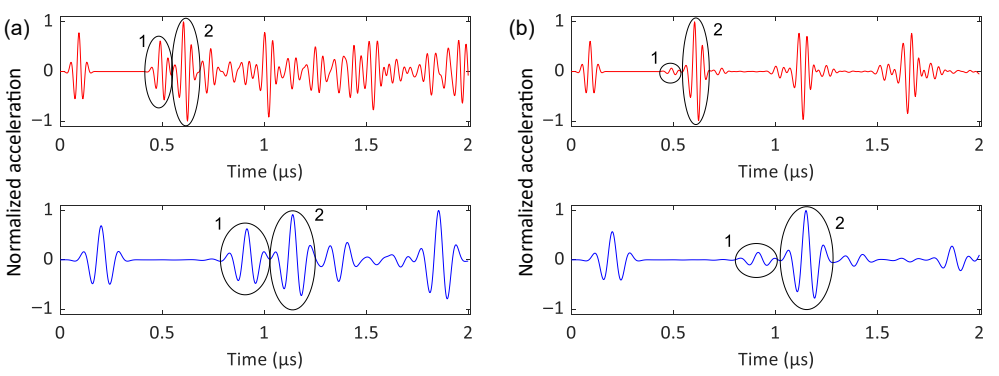


Fig. 5 Comparison of 22 MHz longitudinal wave response and 10 MHz shear wave response: (a) aluminium-coated sample (350 μm coating) and (b) copper-coated sample (250 μm coating).



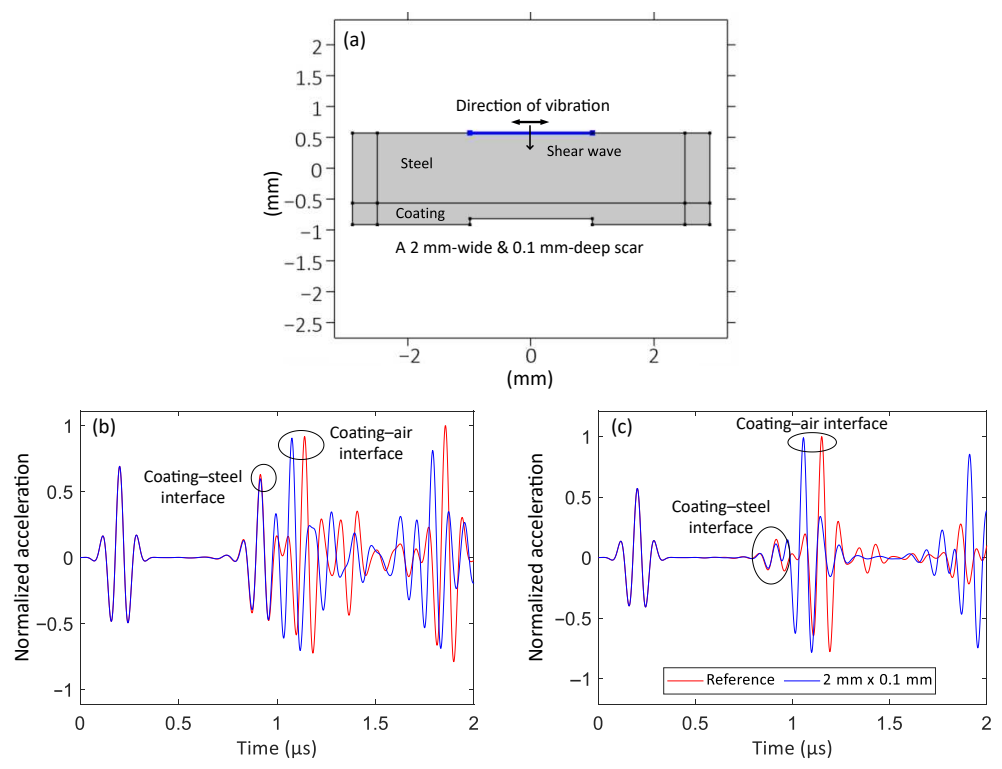


Fig. 6 Simulation using a 10 MHz shear wave to measure a 2 mm-wide, 0.1 mm-deep wear: (a) diagram of simulation; (b) simulation results of aluminium coated sample; (c) simulation results of copper coated sample.

0.1 mm-deep independent scar. In Fig. 8(a), the energy of the shear wave is partially reflected to both sides, while longitudinal waves have been mainly reflected toward the sensor, with only a small amount of energy reflected to other directions, as shown in Fig. 8(b).

Based on the simulation results, the shear waves propagation in a double-layer structure is similar to that of longitudinal waves, exhibiting as two adjacent reflections from both interfaces of the coating. Compared with longitudinal waves, shear waves show a larger ToF between the two interfaces, indicating a better resolution. In addition, shear waves are more sensitive to discontinuous scars, typically displayed as a decrease in the amplitude of the coating-air interface reflection. For example, a significant change in amplitude without a shift in peak position can indicate a slight wear on the surface.

4 *In-situ* measurement of bearing coatings

4.1 Shear waves speed of sound calibration

To test the performance of ultrasonic shear waves for coating thickness and wear measurement, a series of *in-situ* tests were carried out on aluminum-alloy coated and bronze-lead coated bearing shells. The shells were instrumented with DL-50HD shear wave sensors. Before testing, the relationship between shear wave speed and temperature was calibrated in a temperature-controlled oven using the same materials. Thermal expansion was ignored because the same batch of shells were used both for calibration and measurement. The results are shown in Fig. 9.

The speed of shear wave variation with temperature for these three materials was fitted using the quadratic relations via Eqs. (8)–(10):

$$c_{\text{Al(s)}} = -0.004289T^2 - 0.3098T + 3,017 \tag{8}$$

$$c_{\text{Bz-Pb(s)}} = -0.001987 \, T^2 - 0.2591T + 1,884 \tag{9}$$

$$c_{\text{Steel(s)}} = -0.002227T^2 - 0.1236T + 3{,}155 \tag{10}$$

4.2 *In-situ* measurement of metallic coatings

A series of *in-situ* measurements was conducted. The rotation speed was set to 600 r/min, with a dynamic load applied during the test. The bearings were lubricated at the start of the operation, but the lubrication was drained halfway to accelerate wear of the coating. The *in-situ* tests for each sample were stopped if the bearing temperature exceeded 120–130 °C or if the shaft seized. The test platform and ultrasound *in-situ* testing system are shown in Fig. 10.

During measurement, three ultrasound sensors were instrumented onto the bearing shell and mounted to the tribometer through a bespoke bearing holder. Two K-type thermocouples were used to monitor the temperature of the bearing shell, located between sensors 1 and 2, and between sensors 2 and 3, clamped between the shell and holder, as shown in Fig. 10(b). The average temperature measured by the thermocouples was used to calculate the real-time speed of shear waves.

4.3 Results of aluminium-alloy coating

Three aluminum-alloy coated samples were tested on the TE92, a multi-functional tribometer manufactured by Plint Tribology (UK). Results are shown in Fig. 11, with the load during testing over-plotted. The three sensors collected the data sequentially. For each sensor, 50 A-scans were recorded every 10 s. The averaged signal of 50 A-scans was used to calculate the ToF and reduce random noise. For example, the averaged signals of aluminium-alloy coated sample 1 are shown in Fig. 11(a). Note that the input signal (at 1 μs) was cut off because the reflections were too weak



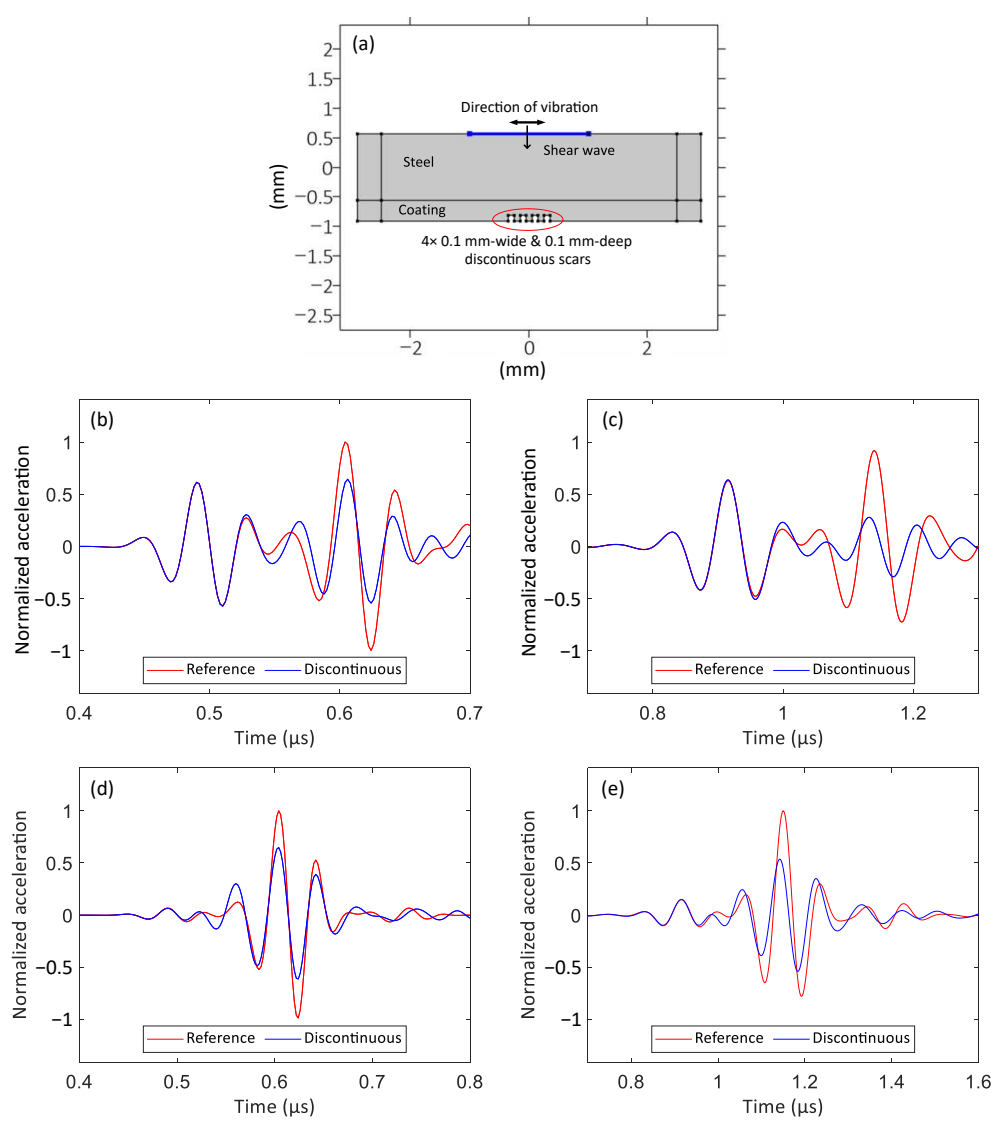


Fig. 7 (a) Diagram of simulation (4 0.1 mm-wide, 0.1 mm-deep scars on 350 μm-thick aluminium coatings). Simulation results of aluminium coated sample: (b) 22 MHz longitudinal wave and (c) 10 MHz shear wave. Simulation results of copper coated sample: (d) 22 MHz longitudinal wave and (e) 10 MHz shear wave.

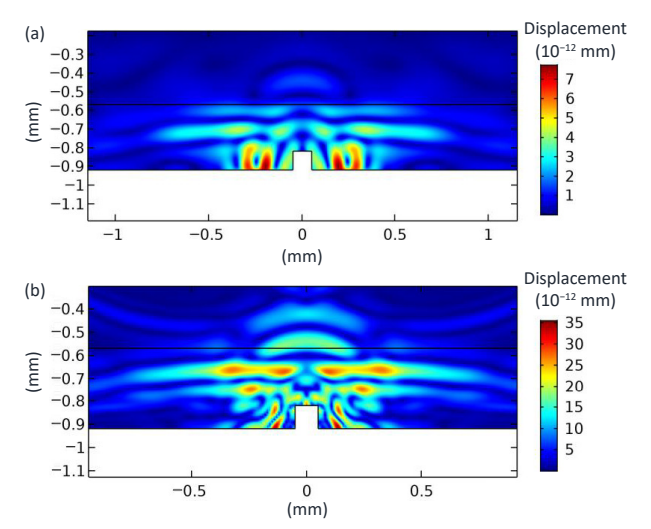


Fig. 8 Simulation results of ultrasonic bulk wave reflection at a 0.1 mm-wide, 0.1 mm-deep independent scar: (a) shear wave and (b) longitudinal wave.

compared with the input. During wear progress, the reflection of the coating-lubricant interface shifts leftwards. As the temperature increases, both coating-steel and coating-lubricant reflections shift rightwards and attenuate slightly.

In Figs. 11(c), 11(e), and 11(g), the temperature was obtained from a thermocouple on the TE92, which monitored the temperature of entire bearing system (chamber and internal lubricant) during operation. This corresponds to the temperature rise stage measured by the thermocouples in the ultrasound system, as shown in Figs. 11(b), 11(d), and 11(f).

Comparing the results of the temperature and ultrasound system, both curves show the same trend. However, after the oil was drained, the local temperature of the bearing shell, especially the contact area, rapidly increased, as indicated on the plot in Fig. 11. Thus, the temperature measured by the ultrasound system is higher than the maximum temperature measured by the TE92.

As the wear progressed in Fig. 11, significant degradation of the coating surface occurred in three stages. The first stage is the lubricated stage, where the entire bearing system was hydrodynamically lubricated, with no significant change in coating thickness and a gentle increases of temperature. In the second stage, most of the lubricant was drained out; the entire bearing system was in a mixed or boundary lubricated region, and the load was reduced to maintain system operation. In this case, the thickness of the coating began to decrease, while the

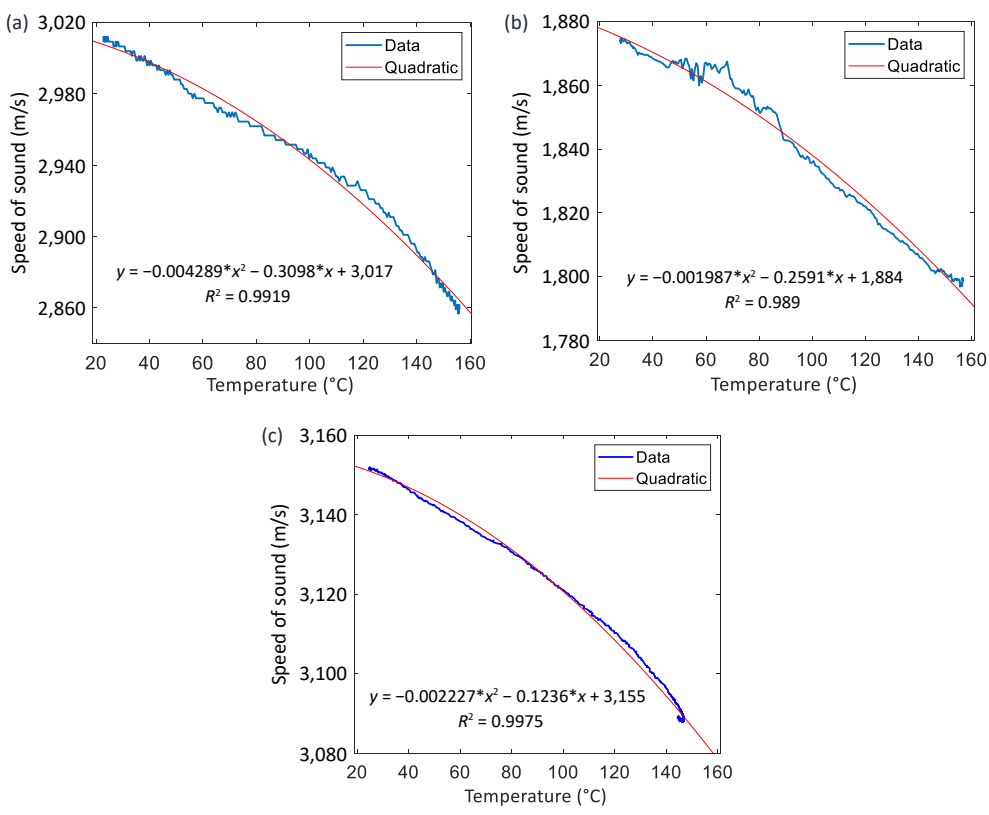


Fig. 9 Speed of shear wave variation with temperature for (a) aluminum-alloy, (b) bronze–lead, and (c) bearing steel.

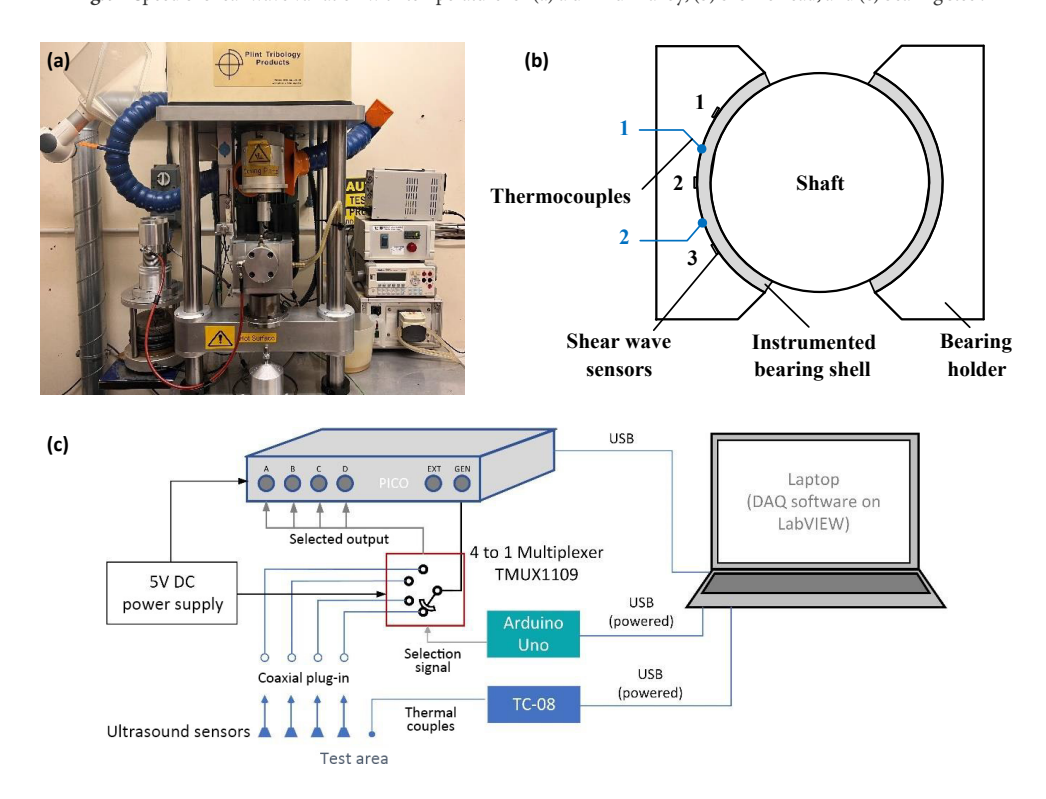


Fig. 10 (a) Rotary tribometer Phoenix TE92. (b) Assembly of tested bearing samples. (c) Diagram of in-situ ultrasound bearing shell measurement system.

temperature increased continuously due to frictional heating. The third stage is the cooling stage, where the machine stopped, and the coating thickness remained unchanged.

For sample 2 sensor 2, after the lubricant drained out, the thickness monitored by the sensor started to increase, and a slight decrease during cooling. This may be due to two reasons. The first

one is that the sensor performance was affected by high temperatures, resulting in a decrease in signal accuracy. The second is that in the tested area, the material extrusion led to a deformation, where the material is extruded to both sides due to the friction. This deformation typically results in an uneven surface, with thinner layers in the middle and thicker layers on



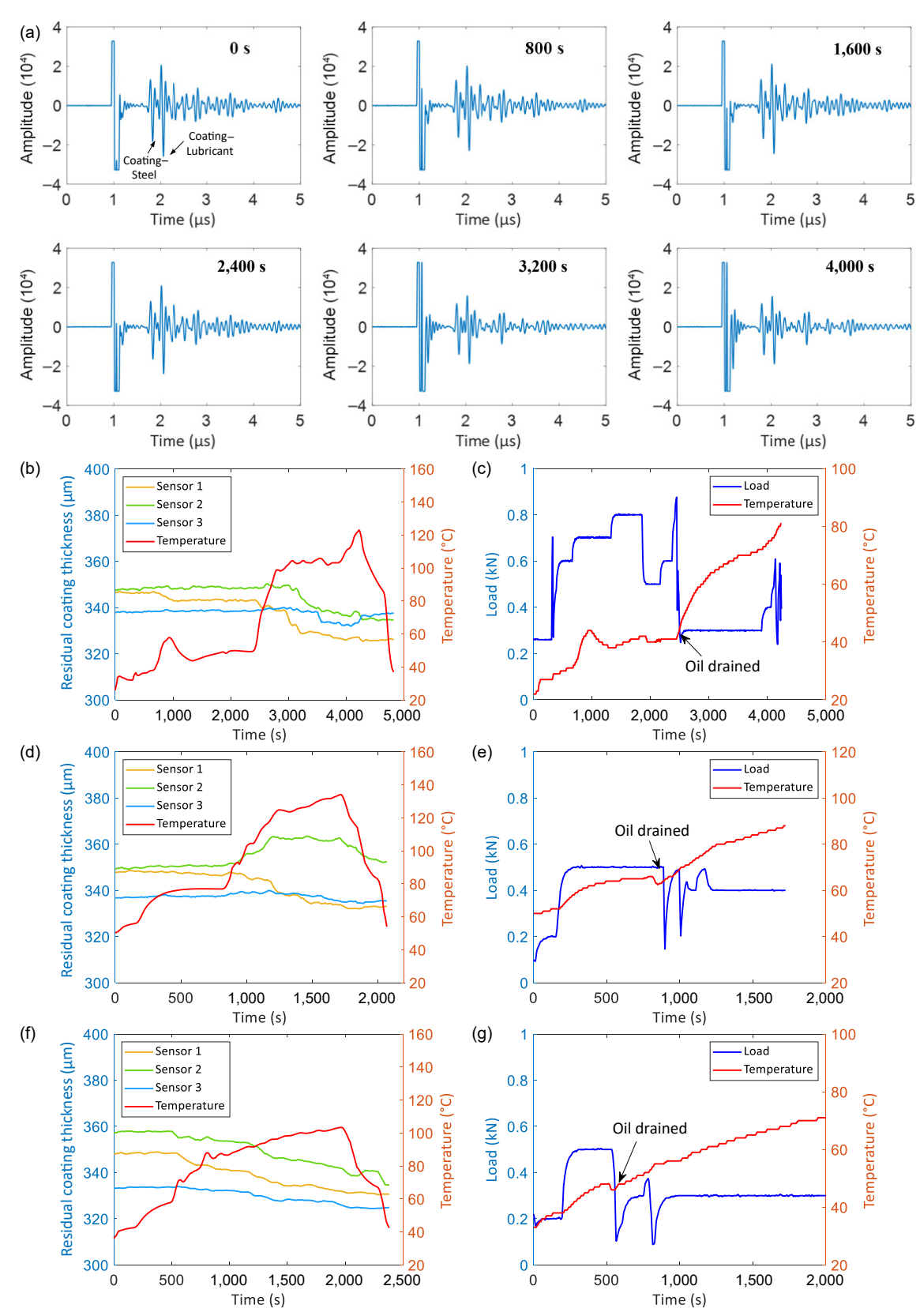


Fig. 11 (a) Ultrasound signal of sample 1. Progression of wear expressed as residual coating thickness and load during measurement for aluminium-alloy coated samples: (b, c) sample 1, (d, e) sample 2, and (f, g) sample 3.

both sides. In such cases, ultrasound may show a larger thickness reading than usual. Figure 12 shows the coating surface under sample 2 sensor 2.

Table 2 compares the ultrasonic shear wave measurement with

microscope images from cross sections. For all three aluminum-alloy coated samples and nine shear wave sensors, the maximum deviation between shear wave and microscope results is $5.13 \mu m$ (sample 1 sensor 3). For the other eight sensors, the deviations are



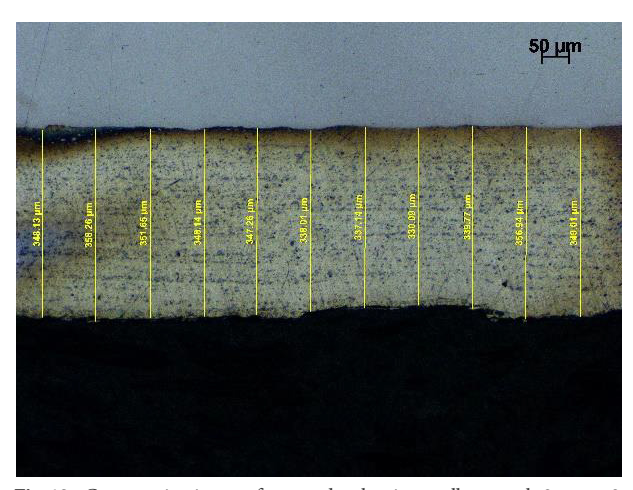


Fig. 12 Cross-section image of area under aluminum-alloy sample 2 sensor 2.

Table 2 Comparison between ultrasonic shear wave measurement and microscope results for aluminium-alloy coated samples

(a) Results of a	aluminum-allo	y coated sample	1		
	Sensor 1	Sensor 2	Sensor 3		
Thickness, start (µm)	346.68	347.66	337.97		
Thickness, end (µm)	326.23	334.69	337.52		
Microscope result (μm)	329.14	337.55	342.65		
Deviation (µm)	2.92	2.87	5.13		
Relative error	0.89%	0.85%	1.50%		
Depth of wear (µm)	20.46	12.97	0.45		
(b) Results of aluminum-alloy coated sample 2					
	Sensor 1	Sensor 2	Sensor 3		
Thickness, start (µm)	347.97	349.53	336.85		
Thickness, end (μm)	332.95	352.76	335.32		
Microscope result (μm)	335.89	352.15	338.51		
Deviation (µm)	2.94	0.61	3.19		
Relative error	0.88%	0.17%	0.94%		
Depth of wear (µm)	15.02	-3.23	1.52		
(c) Results of aluminum-alloy coated sample 3					
	Sensor 1	Sensor 2	Sensor 3		
Thickness, start (μm)	348.33	357.57	333.24		
Thickness, end (µm)	330.57	337.06	324.65		
Microscope result (μm)	334.86	336.28	324.25		
Deviation (µm)	4.29	0.78	0.41		
Relative error	1.28%	0.23%	0.13%		
Depth of wear (µm)	17.76	20.51	8.58		

within 5 μ m. Thus, the ultrasonic shear waves show good accuracy for the *in-situ* measurement of aluminum-alloy coated bearings.

4.4 Results of bronze-lead coating

Three bronze–lead coated samples have also been tested. The progression of wear during *in-situ* measurement and the dynamic load are shown in Fig. 13. Sample 1 sensor 2 shows an abnormal decrease, possibly due to the high temperature after the drainage of lubricant, as shown by the green line in Fig. 13(a). The wear progress of the area under sample 2 sensor 2 is similar to that of aluminum-alloy coated sample 2 sensor 2. Figure 13(e) shows almost no wear on sample 3. The microscope results indicate only very slight deformation at the tested positions.

Table 3 compares the ultrasonic shear wave measurement with

microscope results for bronze–lead coated samples. The result shows good performance of these shear wave sensors. Only the deviation for sample 1 sensor 3 exceeds 5 μ m (5.54 μ m, 2.51% error). Overall, the performance of ultrasonic shear wave sensing on the bronze–lead coating is also satisfactory.

5 Discussion

5.1 Amplitude reduction of reflected waves

The propagation of ultrasonic shear wave was studied using the finite element method. It shows that when the shear waves encounter discontinuous scars, the amplitude of reflected signals attenuates significantly. Therefore, the roughness or surface deformation of the coating may be estimated from the ratio of the amplitudes of the reflected signals from either side of the coating. The amplitude ratio R is given by Eq. (11), where A_1 is the amplitude of coating-steel reflection and A_2 is the amplitude of coating-lubricant reflection. This phenomenon is more explicit for aluminium-alloy coated samples, as reflections from the two interfaces are nearly at the same level. Results for aluminium-alloy coated samples are shown in Fig. 14.

$$R = \frac{A_1}{A_2} \tag{11}$$

As shown in Fig. 14, the amplitude ratio of the coating-steel reflection to coating-lubricant reflection is between 0.55 and 0.65 at the start. When temperature increases, i.e. frictional heating occurred, the amplitude ratio increases, as marked in Figs. 14(a)–14(c). This means a decrease in the amplitude of the coating-lubricant reflection, indicating the surface was discontinuous at that time.

In Figs. 14(a) and 14(b), a short period without temperature change shows an unchanged amplitude ratio, indicating no surface damage at that time. Figure 14(d) shows a comparison between the reflected signals at the start and during friction. Moreover, the amplitude ratio for sample 2 sensor 2 and sample 3 sensor 2 (green lines in Figs. 14(b) and 14(c)) shows an alternating rising-falling trend. It can be speculated that the surface in that area experienced an alternately rough-smooth progression. More surface profile information could potentially be obtained using both longitudinal and shear waves, such as the early deformation before material loss.

5.2 Further research

The main purpose of this work is to propose an *in-situ* wear measurement solution of metallic coated journal bearing shells using active ultrasonic shear wave. The future research will mainly focus on the enhancement of accuracy, where shear wave speed and ToF are key factors affecting the pulse-echo method.

Accurate real-time shear wave speed during measurement is crucial. In this work, the shear wave speed in steel substrate and coating materials is calibrated in advance, and changes during material heating are studied. In practical applications, the bearing shell temperature variations are complex, and under boundary lubrication conditions, the temperature at the solid contact may increase rapidly. For example, according to Eq. (10), for bronze–lead coatings, if the measured temperature (130 °C) is lower than the actual value (140 °C), due to the delayed temperature sensor response, the error introduced was approximately 1.9 μm . With more friction and wear, the error increases.

Moreover, for large-sized shells, the variation in the speed of



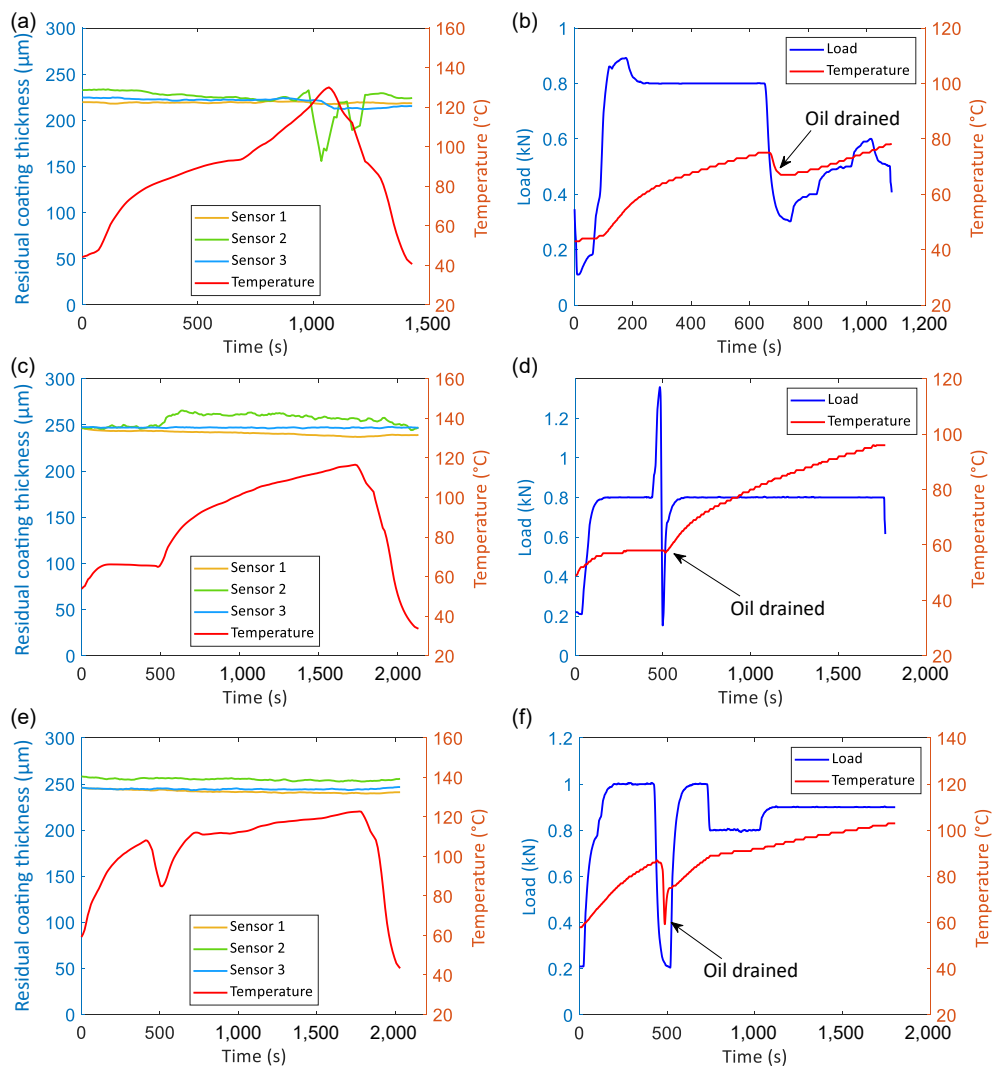


Fig. 13 Progression of wear expressed as residual coating thickness and dynamic load during measurement for bronze-lead coated samples: (a, b) sample 1, (c, d) sample 2, and (e, f) sample 3.

sound gradient was required to be considered [17, 18]. According to previous tests on a 7 mm-thick Bz–Pb coated plate, the temperature difference between both plate surfaces was 4.5 °C, leading to an error of approximately 1 µm. Therefore, a temperature compensation strategy will be further investigated, especially for large components, such as marine bearing samples. A self-calibration strategy using both longitudinal and shear sensors may compensate for the internal temperature gradient. Additionally, the shear wave speed is also affected by pressure. Local density changes of material necessitate considering the pressure influence on shear wave speed during future calibration.

ToF is another important factor, enabling a higher time and spatial resolution in actual measurement. The performance of higher ultrasonic shear wave frequencies, as high as the longitudinal wave frequencies, was investigated. The longer ToF of the shear wave means a higher resolution when the sampling rate is constant. A 22 MHz shear wave was compared with a 22 MHz longitudinal wave via simulation, as shown in Fig. 15. The red curve represents the response of the longitudinal wave, and the blue curve represents the response of the shear wave. The pulses 1 and 2 marked in these figures represent the coating-steel and coating-air reflection respectively. The blue curve shows two distinctive reflections, each more compact than the 10 MHz shear wave pulses. With advancements in piezo-element manufacture,

higher frequency shear wave sensors are being developed, expected to replace longitudinal wave sensors for real-time monitoring.

6 Conclusions

In this study, ultrasonic shear wave measurement of metallic coating thickness and wear has been evaluated. Simulations and *insitu* experiments have proved the feasibility of shear wave sensing to determine wear on coated bearing shells. Based on the simulation results, it has been shown that shear waves have a similar behavior to longitudinal waves in a double-layer structure, where two reflections from the interfaces either side of the coating and the thickness of coating can be obtained from the ToF. Comparing the 10 MHz shear wave and 22 MHz longitudinal wave response, it was shown that the 10 MHz shear wave is suitable for wear measurement. The simulation also showed shear waves are more sensitive to discontinuous wear scars, while the shear wave measurement of a bearing shell is shown in Fig. 16.

In-situ shear wave measurements of bearing coating wear were carried out and the results show that shear wave measurement align with the microscope results. For three aluminum-alloy coated samples and nine shear wave sensors, there is a maximum deviation of 5.13 µm (sample 1 sensor 3). For the other eight



Table 3 Comparison between ultrasonic shear wave measurement and microscope results for bronze-lead coated samples

	(a) Results of bronze-lead coated sample 1						
	Sensor 1	Sensor 2	Sensor 3				
Thickness, start (μm)	219.53	233.10	224.46				
Thickness, end (μm)	218.35	224.83	215.00				
Microscope result (μm)	221.66	227.42	220.54				
Deviation (µm)	3.32	2.59	5.54				
Error	1.50%	1.14%	2.51%				
Depth of wear (µm)	1.19	8.27	9.47				
	(b) Results of bronze-lead of	coated sample 2					
	Sensor 1	Sensor 2	Sensor 3				
Thickness, start (μm)	245.23	246.68	247.59				
Thickness, end (μm)	238.93	247.37	247.10				
Microscope result (μm)	238.36	248.81	247.55				
Deviation (µm)	0.56	1.44	0.45				
Error	0.24%	0.58%	0.18%				
Depth of wear (µm)	6.30	-0.69	0.49				
	(c) Results of bronze-lead of	oated sample 3					
	Sensor 1	Sensor 2	Sensor 3				
Thickness, start (μm)	245.24	257.42	245.43				
Thickness, end (μm)	240.75	254.67	246.13				
Microscope result (μm)	241.26	257.63	248.68				
Deviation (µm)	0.52	2.96	2.55				
Error	0.21%	1.15%	1.03%				
Depth of wear (μm)	4.49	2.75	-0.70				

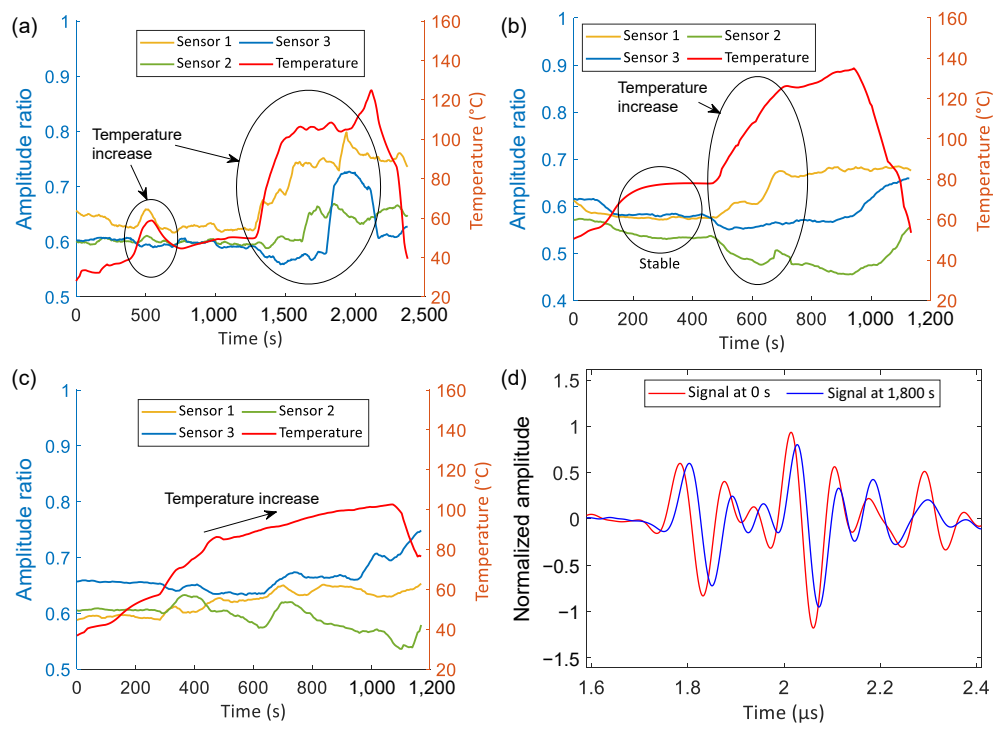


Fig. 14 Amplitude ratio of coating-steel reflection to coating-lubricant reflection during *in-situ* measurement for aluminium-alloy coated samples: (a) sample 1, (b) sample 2, and (c) sample 3. (d) Comparison of ultrasound reflection between signals collected at start and during friction.



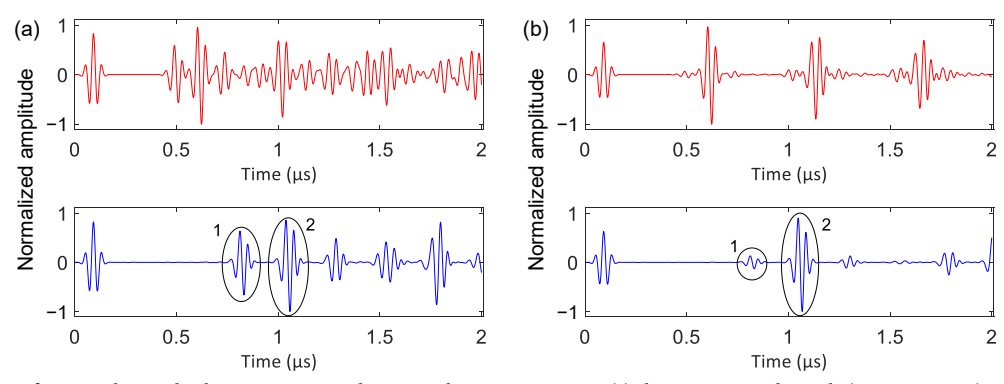


Fig. 15 Comparison of 22 MHz longitudinal wave response and 22 MHz shear wave response: (a) aluminium coated sample (350 μm coating) and (b) copper coated sample (250 μm coating).

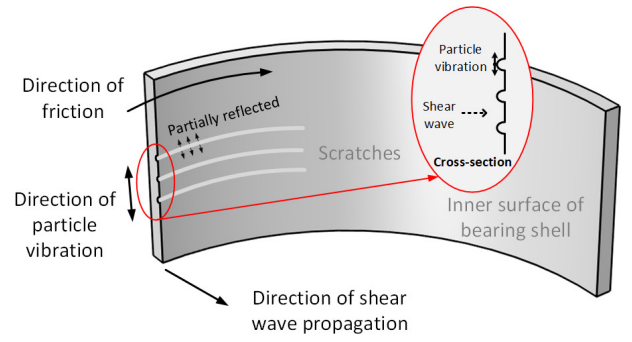


Fig. 16 Ultrasonic shear wave measurement in bearing shell.

sensors, the deviations are within 5 μ m. For the bronze–lead coatings, only the deviation of sample 1 sensor 3 exceeds 5 μ m (5.54 μ m, 2.51% error). The progression of the wear during the test of these samples has been plotted.

Shear wave sensing is simultaneously expected to enable the estimation of the roughness of the coating surface. If the shear sensor with higher frequency can be manufactured, the shear wave measurement may replace the longitudinal wave measurement for the thin coatings.

Acknowledgements

The authors would like to acknowledge the financial support of the Daido Metal Co. that funded this work. R. S. Dwyer-Joyce would also like to acknowledge the financial support of the Engineering and Physical Sciences Research Council through his fellowship on Tribo-Acoustic Sensors EP/N016483/1.

Declaration of competing interest

The authors have no competing interests to declare that are relevant to the content of this article.

References

- Jin S J, Wang Z C, Yang Y N, Luo Z B. Corrected mode-converted wave method for detecting defects in TOFD dead zone. *J Nondestruct Eval* 42(3): 62 (2023)
- [2] Lee H, Kim K, Lee Y. Development of stiffness measurement program using color mapping in shear wave elastography. *Diagnostics* 10(6): 362 (2020)
- [3] Zhang J, Song Y F, Li X B, Zhong C H. Comparison of experimental measurements of material grain size using ultrasound. J Nondestruct Eval 39(2): 30 (2020)
- [4] Song P F, MacDonald M, Behler R, Lanning J, Wang M, Urban M, Manduca A, Zhao H, Callstrom M, Alizad A, Greenleaf J F, Chen S G. Two-dimensional shear-wave elastography on conventional ultrasound scanners with time-aligned sequential tracking (TAST)

- and comb-push ultrasound shear elastography (CUSE). *IEEE T Ultrason Ferr* **62**(2): 290–302 (2015)
- [5] Kim N Y, Lee S S. Elastic property measurement of high-tension bolt based on mode converted ultrasound. *Key Eng Mater* 326–328: 709–712 (2006)
- [6] Kim N, Hong M. Measurement of axial stress using mode-converted ultrasound. NDT E Int 42(3): 164–169 (2009)
- [7] De Araújo Freitas V L, de Albuquerque V H C, de Macedo Silva E, Almeida Silva A, Tavares J M R S. Nondestructive characterization of microstructures and determination of elastic properties in plain carbon steel using ultrasonic measurements. *Mater Sci Eng A* 527(16–17): 4431–4437 (2010)
- [8] Bustamante L, Saeki M, Matsukawa M. Characterization of shear waves in cortical bone using the axial transmission technique. *Jpn J Appl Phys* 58: SGGE20 (2019)
- [9] Salinas V, Aguilar C, Espinoza-González R, González J, Henríquez J, Lund F, Mujica N. *In-situ* monitoring of dislocation proliferation during plastic deformation of 304L steel using ultrasound. *Mater Sci Eng A* 849: 143416 (2022)
- [10] Dang G, Pei C X, Yang Z F, Zhou H Q. Residual strain measurement based on longitudinal to shear wave velocity ratio with a dual-mode EMAT. *Front Mater* **10**: 1273190 (2023)
- [11] Zhao Y, Ma J, Chen J W, Ouyang H, Wang M H, Zhao P, Zhang B. Noncontact method applied to determine thickness of thin layer based on laser ultrasonic technique. *Mater Res Innov* 18: S2-1081–S2-1085 (2014)
- [12] Parra-Raad J, Khalili P, Cegla F. Shear waves with orthogonal polarisations for thickness measurement and crack detection using EMATs. NDT E Int 111: 102212 (2020)
- [13] Wu L Q, Palamarciuc I, Bajwa R, Zhang Y, Dwyer-Joyce R. Ultrasonic measurement for surface damage monitoring in coated bearing shells. *Friction* **13**(9): 9441065 (2025)
- [14] Wu L Q, Palamarciuc I, Bajwa R, Zhang Y, Dwyer-Joyce R. The wear measurement of journal bearing coatings that are poor reflectors using ultrasound analytical signals. *Wear* 572: 206052 (2025)
- [15] Rose J L. Ultrasonic Guided Waves in Solid Media. Cambidge (UK): Cambidge University Press, 2014.
- [16] Gammell P M. Improved ultrasonic detection using the analytic signal magnitude. *Ultrasonics* 19(2): 73–76 (1981)
- [17] Jia Y P, Wu T H, Dou P, Yu M. Temperature compensation strategy for ultrasonic-based measurement of oil film thickness. Wear 476: 203640 (2021)
- [18] Jia Y P, Dou P, Zheng P, Wu T H, Yang P P, Yu M, Reddyhoff T. High-accuracy ultrasonic method for in situ monitoring of oil film thickness in a thrust bearing. Mech Syst Signal Process 180: 109453 (2022)





Liqun Wu is currently on a lectureship at Tianjin University of Science and Technology. He received his B.Eng. degree at Tianjin University (2016) and M.Sc. degree at Tianjin University of Science and Technology (2019). He did his Ph.D. work in tribology at the University of Sheffield, funded by Daido Metal. His research area involves the non-destructive testing and intelligent measurement systems, especially ultrasound and vision measurement.



Ion Palamarciuc is a senior R&D engineer at Daido Metal, with a Ph.D. degree in materials engineering from Gheorghe Asachi Technical University of Iasi, Romania. His research focuses on the intersection of tribology, material science, and condition monitoring, with extensive expertise in advanced testing methods, such as acoustic emission, destructive, and non-destructive evaluation techniques. With a background in developing coatings,

investigating lubrication regimes, and analyzing wear and friction performance, his research interests include developing innovative solutions for condition monitoring and enhancing material performance in critical applications.



Rizwan Sarwar Bajwa is a project manager/PMO at the ENERCOMP (ARAMCO-KAUST Consortium for Nonmetallics and Composites in Energy Applications), Mechanics of Composites for Energy and Mobility Laboratory (MCEM), PSE Division, KAUST, KSA. Before joining KAUST in 2024, he served as R&D manager at the European Technical Centre (UK) for DAIDO METAL Co., Ltd., where he led company's research and development efforts

focusing on high-performance products, materials, and innovative technologies for the automotive, marine, and energy sectors. Expert in leading cross-functional teams, driving product development from concept to commercialization. He finished his Ph.D. degree at Bournemouth University (UK), fully sponsored by Schaeffler Technologies GmbH & Co. KG, Germany. After the completion of his Ph.D. degree, he joined DAIDO METAL CO., LTD., European Technical Centre (UK) in 2016.



Yi Zhang received his Ph.D. degree in materials engineering at Loughborough University in 2007. After the completion of his Ph.D., he joined Daido Metal Co. Ltd., European Technical Centre, UK, as a materials scientist in 2007, becoming a principal materials scientist and head of R&D in 2013 and 2015, leading the research activities in UK. Since 2022, he has worked in the corporation headquarters in Japan. His research interests cover a wide range

of areas such as material science, surface engineering & manufacturing, tribology, and most recently, emerging technologies.



Rob S. Dwyer-Joyce, professor, is director of the Leonardo Centre for Tribology at the University of Sheffield. He has a first degree in mechanical engineering and did his Ph.D. in tribology at Imperial College London. He pioneered the use of ultrasound for tribological machine elements to measure oil film, contact load, and viscosity. He has published over 150 papers in international journals. He was director of the Centre for Doctoral Training in

Integrated Tribology, an EPRSC Advanced Career Fellow, Fellow of the Royal Academy of Engineering, and past editor of the IMechE Journal of Tribology.

